Plasmonic spectra of individual subwavelength particles under the infrared microscope: Cells and airborne dust

James V. Coe*, David B. Lioi, Lindsey Shaffer, Marvin A. Malone, Antriksh Luthra, and Aruna Ravi

The Ohio State University Department of Chemistry and Biochemistry, 100 West 18th Avenue, Columbus OH 43210-1173

ABSTRACT

A plasmonic metal film with a subwavelength hole array (a mesh) is used to capture an individual subwavelength particle, like a single yeast cell or airborne dust particle, and an imaging infrared (IR) microscope, records a scatter-free, IR absorption spectrum of the particle. Individual spectra of wavelength scale particles usually suffer from large scattering effects. This paper starts by demonstrating the plasmonic nature of the mesh in the infrared, proceeds to how this special form of light (surface plasmon polariton mediated transmission resonance) leads to scatter-free IR absorption spectra of individual, subwavelength particles, and ends with work on yeast cells and dust particles from our laboratory air and a household filter.

Keywords: metal film with hole arrays, plasmonic mesh, scatter-free spectra of subwavelength particles, single yeast cell, airborne dust, particulate matter, infrared imaging microscope

1. INTRODUCTION

Plasmonic metal films with subwavelength hole arrays[1, 2] (mesh) can be used to capture an individual subwavelength particle in a hole of the mesh as shown in Figure 1[3]. Such a particle can be examined with an imaging infrared (IR) microscope by either recording a scatter-free, IR absorption spectrum or by the shift it produces in a plasmonic transmission resonance[3-6]. The mesh exhibits "extraordinary transmission"[7, 8] and can be considered a high-tech IR window even though it is made of metal. Meshes have been described as inside-out fiber optics[9] meaning that light is made to run along the surface of the mesh in the form of surface plasmon polaritons. When the polaritons running along the metal surface come to a hole, they interact with the modes of the hole and

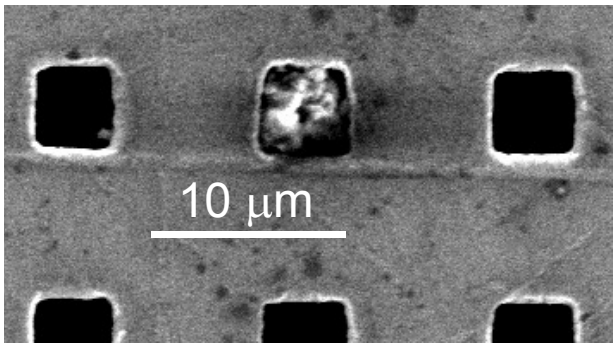

Figure 1. Scanning electron microscope image of airborne dust particle trapped in a hole of our Ni plasmonic mesh (~5μm holes, 12.644 μm lattice parameter, ~2μm thick).

can couple out as light without being scattered from the original beam[10-13], i.e. they can still be detected at a remote spectrometer's detector. Such light has been squeezed through subwavelength holes. By placing sample in these holes and using an imaging microscope, it is possible to isolate the spectra of individual subwavelength particles that have been trapped in the holes[3-6, 14]. Before discussing this application, the plasmonic nature of the mesh will be established. After establishing the plasmonic nature of the mesh, experiments are described which obtain scatter-free IR absorption spectra of individual subwavelength particles. The paper ends with some specific examples including yeast cells and dust from our lab air and a household filter.

*coe.1@osu.edu; phone (614)292-9489; fax (614)292-1685

Plasmonics in Biology and Medicine XI, edited by Tuan Vo-Dinh, Joseph R. Lakowicz, Proc. of SPIE
Vol. 8957, 89570A · © 2014 SPIE · CCC code: 1605-7422/14/$18 · doi: 10.1117/12.2037114

2. PLASMONIC NATURE OF THE MESH

The plasmonic mesh was a special production lot from Precision Eforming (www.precisioneforming.com) in which the usual nickel interior was electrodeposited with an exterior of gold, i.e. a gold plated Ni mesh. The mesh consisted of a square lattice with square-ish holes (~5μm wide holes, 12.644 μm lattice parameter, ~2μm thick, similar to the mesh pictured in Figure 1). Optically speaking, the mesh is a biperiodic grating being used in

transmission mode. At perpendicular incidence, this mesh has a primary resonance at 749 cm^{-1} (13.4 μm) with a transmission of 49% - even though the percentage open area of the holes is only 16%, i.e. it exhibits Ebbesen's extraordinary transmission[7]. It is important to know where resonances lie in reciprocal space relative to the light line in order to characterize their plasmonic nature. Consequently, it is important to know the lattice parameter very accurately so that one knows how close resonances are to the light line as it folds into reciprocal space. Also, the diffraction pattern is intimately related to the identity of specific transmission resonances[15] as is described in the following. A least squares strategy was developed so that multiple diffraction spots contribute to the lattice parameter result.

2.1 Lattice Parameter and Diffraction Spots

The diffraction spot experiment to determine the lattice parameter of our plasmonic mesh is shown in Figure 2. A red laser (λ=632.8 nm) was aligned perpendicular to a screen such that vertical spots were obtained. The position of

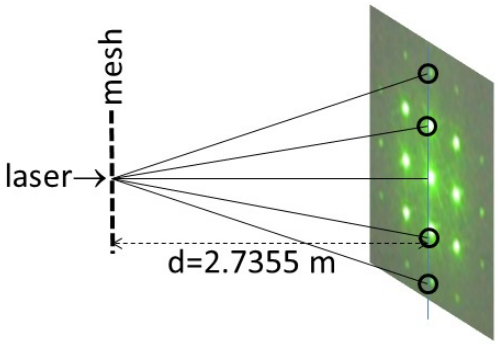

j	m_j	y_j
0	2	0.2749 m
1	1	0.1372 m
		0.0000 m
2	-1	-0.1370 m
3	-2	-0.2752 m

Figure 2. Pictorial depiction of the diffraction spot experiment in which a laser (λ=632.8 nm) was directed perpendicularly through the mesh. The spot positions were measured vertically relative to the (0,0) spot for a given spacing between the mesh and screen.

the circled spots was measured (y_j) relative to the zero order spot as shown in the table in the figure. The spots were indexed by both their vertical index in reciprocal space m_j and an index j over the spots for least squares fitting. The distance, d=2.7355 m, from the mesh to the spot screen was also measured in order to employ a Bragg relation, $Lsin\theta = m\lambda$, where L is the lattice parameter, θ is the scattering angle from the mesh relative to horizontal, m is the reciprocal space step index, and λ is the wavelength. By substituting a hypotenuse and rearranging, one obtains a linear relation $\lambda\sqrt{d^2+y_j^2}/y_j = L/m_j$ where a plot of $\lambda\sqrt{d^2+y_j^2}/y_j$ vs L/m_j has a slope of L, the lattice parameter. With measurements that go from $j = 1,2,\ldots n$, least squares expressions (using all of the measurements) for the lattice parameter, L, and its standard deviation, ΔL , are

$$L = \frac{\sum_j \frac{\lambda\sqrt{d^2+y_j^2}}{m_j y_j}}{\sum_j 1/m_j^2}, \qquad \Delta L = \sigma_y\sqrt{1/\sum_j\left(1/m_j^2\right)}, \qquad \text{and} \qquad \sigma_y = \sqrt{\frac{\sum_j\left[\frac{\lambda\sqrt{d^2+y_j^2}}{y_j} - L/m_j\right]^2}{n-1}}. \qquad (1)$$

The result using the data in Figure 2 was L=12.644±0.005 μm.

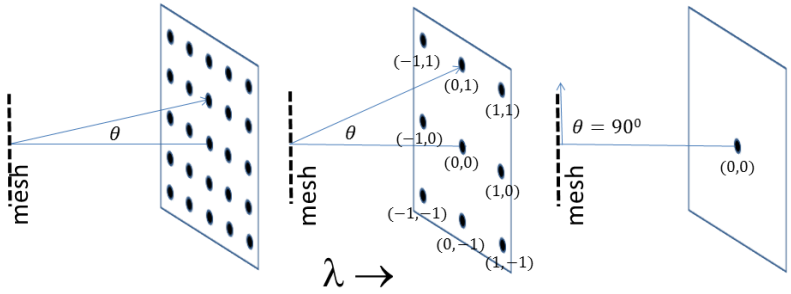

Figure 3. Schematic of diffraction spots showing how the spacing between diffraction spots increases as the wavelength increases. At some specific wavelength, a spot will no longer be transmitted. Instead it propagates parallel to the surface of the mesh as an evanescent wave.

The diffraction spots have a fundamental connection to mesh transmission resonances which is illustrated in Figure 3. The number of diffraction spots that can be observed decreases as the wavelength of light incident on mesh increases. Similarly, the angle with which a diffraction spot exits the mesh also increases with longer wavelength. Transmission resonances arise at wavelengths in which a specific diffraction spot is no longer transmitted. Instead, it propagates along the surface of the mesh as a surface plasmon polariton. Such a mixed state can interact with the holes coupling back out as light. Some of the scattered light rejoins the original beam without being scattered. The plasmonic resonances are labelled by the same (*i,j*) values which identify the corresponding diffraction spots (at shorter wavelengths).

2.2 Dispersion of Transmission Resonances

In the course of developing plasmonic transmission resonances for use under the IR microscope, it was discovered that the rotation of a mesh within the microscope's focal plane and about the optical axis serves as a useful dispersion coordinate[16]. A sample holder with two variable angles was constructed which enabled the mesh to be manipulated simultaneously about the two axis rotation angles, θ and φ, as defined in Figure 4 within the sample

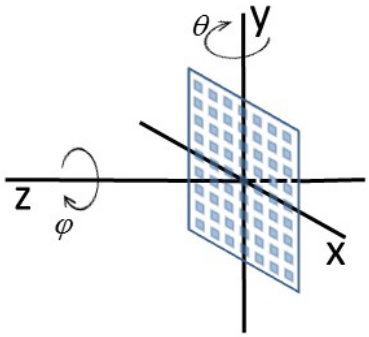

Figure 4. With light incident on the mesh along the z-axis, this schematic defines angles of rotation for dispersion experiments.

region of a benchtop FTIR instrument. Momentum along the mesh surface in the *x*- and *y*-directions is defined by the wavevectors, $k_x = 2\pi\tilde{\nu}sin\theta cos\varphi$ and $k_y = 2\pi\tilde{\nu}sin\theta sin\varphi$, where $\tilde{\nu}$ is the wavenumber of the IR light. When φ=0^0 and θ is varied, one explores the ΓX reciprocal space and when φ=45^0 and θ is varied, one explores ΓM space. In contrast, when θ is fixed and φ is varied, one explores the connection between ΓX and ΓM space, i.e. XM space. Since ΓX and ΓM space of mesh have been explored by us in other work[14, 17], IR transmission spectra of mesh are shown in Figure 5 where θ=28^o and φ is varied from 0-45^o. These spectra were recorded with a Perkin Elmer Spectrum benchtop FTIR system (resolution of 4 cm^{-1}, 500-4000 cm^{-1} range, 150 scans, MCT detector). These spectra exhibit dramatic changes as the ΓX spectrum at φ=0^o transforms into a ΓM spectrum at φ=45^o. A large data set of spectra was recorded by varying both φ and θ effectively exploring the two dimensional momentum space of k_x and

k_y. Transmission peaks were identified by smoothing the spectra and taking 2nd derivatives. Transmission resonance positions (filled circles) as a function of θ and φ are given in Figure 6. Positions of (i,j) resonances are associated with momentum matching surfaces in the two dimensional k_x, k_y space as:

$$\tilde{\nu}_{i,j} = \frac{\frac{sin\theta}{L}(icos\varphi + jsin\varphi) + \sqrt{\left[\frac{sin\theta}{L}(icos\varphi + jsin\varphi)\right]^2 + \frac{(n^2-(sin\theta)^2)}{L^2}(i^2+j^2)}}{n^2-(sin\theta)^2}, \qquad (2)$$

where n is the effective index of refraction. The lines in Figure 6 correspond to n=1.000, i.e. they reveal how the light surfaces fold as lines into this reduced reciprocal space. Many resonances follow the light lines closely and

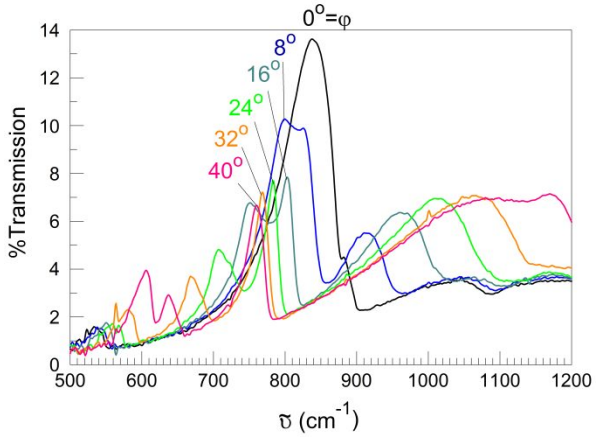

Figure 5. IR transmission spectra of gold plated Ni mesh with θ fixed at 28°. The dramatic changes reveal the transformation of a ΓX spectrum at φ=0° to a ΓM spectrum at φ=45°.

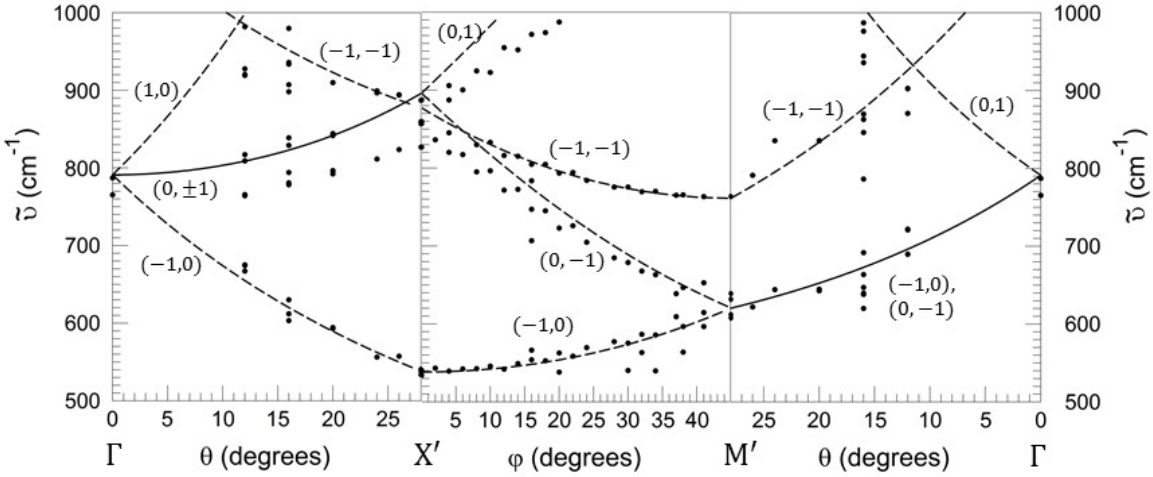

Figure 6. Dispersion diagram mapping the position of transmission resonances in ΓX space as φ=0° and θ=0-28° (left panel), XM space as φ=0-45° and θ=28° (middle panel), and MΓ space as φ=45° and θ=28-0° (right panel). The lines are light lines which fold into the reciprocal space.

there are band gaps at the crossings of lines showing that the resonances interact with each other (pushing off of the light lines). The solid lines in Figure 6 indicate intersecting seams, i.e. places where two different (i,j) resonances are degenerate along a line. In this case, as with the (0,±1) resonance in the ΓX' panel, an interaction (splitting of ~50 cm^{-1}) is exhibited along the whole stretch of this line. The dispersion diagram of Figure 6 is not unlike that which might be made for a photonic crystal[18] (see p 136). The primary difference is that we cannot acquire data all the way to θ=90°, so this plot stops at θ=28°. Instead of getting all the way to the X and M points in reciprocal space, we get to points called X' and M' that correspond to θ=28°. The left panel has φ fixed at 0° (part of ΓX), while the right panel has φ fixed at 45° (part of ΓM). The middle panel has θ fixed at 28°, while φ is varied. It shows the connection

between the ΓX and ΓM planes. In order to have rectangular panels, the data are plotted vs θ and φ rather than k_x and k_y. By searching regions away from the high symmetry ΓX and ΓM areas, we discovered some very narrow resonances (~9 or 10 cm^{-1}) as shown in Figure 7.

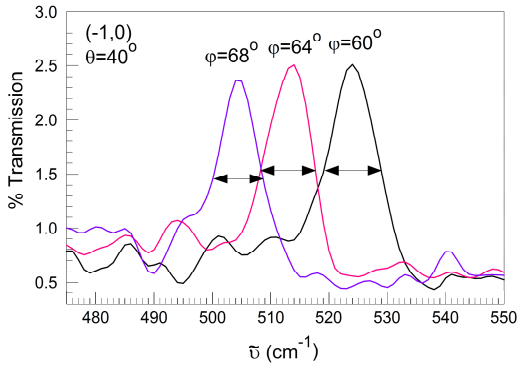

Figure 7. Narrow transmission resonances obtained at θ=40° and φ=60, 64, and 68°.

3. THE INFRARED MICROSCOPE FOR PLASMONIC SENSING AND SPECTRA

The optics of an IR microscope are very different than those of a benchtop FTIR as shown at the top of Figure 8. In the microscope, a cone of light is focused onto the object such that no light rays are perpendicularly incident

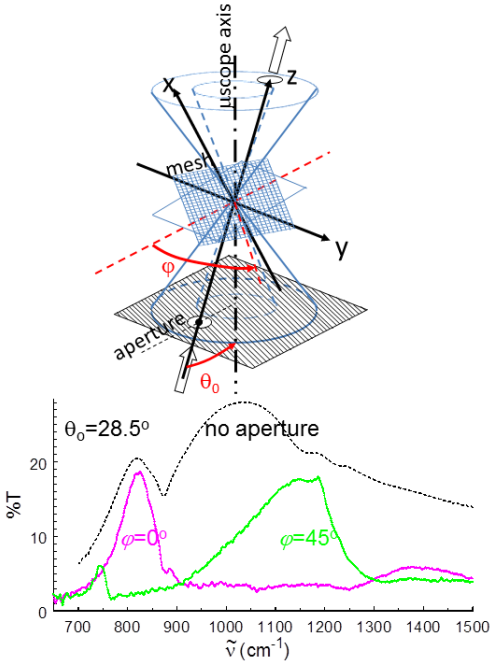

Figure 8. (top) Schematic of mesh in the IR microscope showing an off-axis aperture which reduces the range of angles. (bottom) Spectra recorded with the aperture at two different mesh rotations and without the aperture.

(Cassegrain optics). The large range of θ and φ angles produces extensive dispersion and averaging of the plasmonic transmission resonances as shown in the dashed spectral trace (bottom of Figure 8) with a label "no aperture". The plasmonic resonances can be observed again by adding an off-axis aperture below the focal plane[16]. With such an aperture, the rotation of the mesh relative to the aperture is important as shown by the lower spectral traces in Figure 8 (labelled "φ=0°" and "φ=45°"). The Perkin Elmer Spotlight 300 system has an average value of θ~28.5° when kept to the maximum of transmission. Rotation of mesh about the microscope axis by φ becomes a dispersion coordinate -

the same dispersion coordinate that was described earlier as connecting ΓX to ΓM in reciprocal space. With the off-axis aperture addition and the use of plasmonic mesh, the IR microscope can be used to examine the effect of particles and microconstructions on plasmonic resonances, i.e. by sensing the shifts of the resonant positions[14]. While work continues on these phenomena, our most important applications to data involve the recording of spectra of individual particles that have been placed in the mesh holes. In fact the averaging of dispersed resonances that comes with the large range of angles in the IR microscope without an aperture makes for a very good background for recording spectra.

4. SUBWAVELENGTH PARTICLES UNDER THE IR MICROSCOPE

Previously it was demonstrated that IR modes mediated by surface plasmon polaritons run rampant across the surface of our plasmonic mesh. A particle in a subwavelength mesh hole experiences radiation very differently than an isolated particle. Light incident on an isolated, wavelength-scale particle is dominated by scattering as is well-modelled by Mie theory[19, 20] (dominant scattering, distorted vibrational lineshapes). A particle in a mesh hole is touched on four sides by surfaces carrying evanescent waves. The mesh spectra are dominated by absorption and are free of the usual Mie scattering effects. Using the same conditions with a Perkin Elmer Spotlight 300 imaging FTIR microscope, spectra of twenty individual 5 μm diameter latex (polystyrene) spheres were averaged as shown in the top of Figure 9, while nineteen single spectra of latex microspheres in mesh holes were averaged to obtain the spectrum in the bottom panel of Figure 9[6]. The plasmonic mesh greatly reduces the amount of scattering as well as the lineshape distortions associated with isolated particles of wavelength scale, however there are many other challenging problems when the strength of vibrational transitions becomes comparable to the geometric cross section of a particle[21].

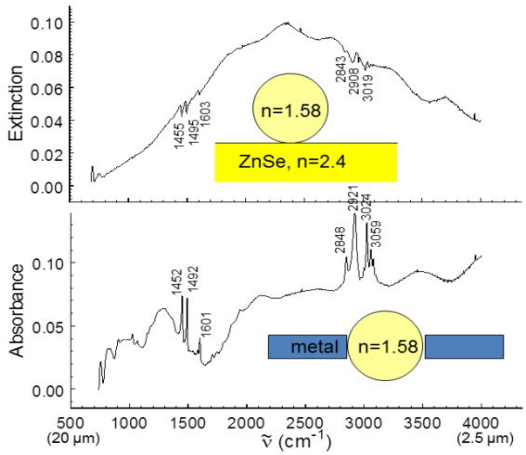

Figure 9. IR spectra of single 5 μm diameter latex (polystyrene) sphere on a ZnSe window (top) and within a hole of metal micromesh (bottom). Dominant scattering effects are diminished by plasmonic mesh.

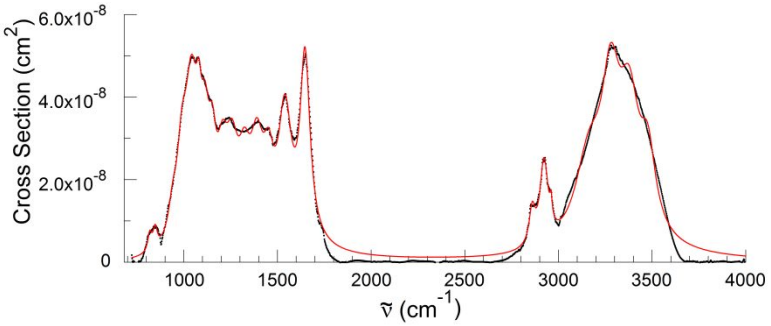

Figure 10. Average IR spectra of 21 individual yeast cells converted to absolute intensities (cross section units) and fit with a Mie model.

It turned out that live bread yeast cells (Saccharomyces cerevisiae) were very easy to get into the 5 μm holes of our plasmonic mesh. The spectra of 21 different individual yeast cells[5, 22] trapped in mesh holes were recorded, averaged, and flattened (approximately spherical objects have lensing effects that reduces signal for shorter wavelengths) as

presented in Figure 10. A calibration based on latex spheres of known size enabled the conversion of absorption to absolute cross section. The spectrum was fit using Mie theory and a complex index of refraction expression with a term for each vibration

$$\boldsymbol{m} = \sqrt{\boldsymbol{\epsilon} + \sum_{\boldsymbol{j}} \frac{\boldsymbol{A_j \tilde{\nu}_{0,j}^2}}{\tilde{\nu}_{0,j}^2 - \tilde{\nu}^2 - \boldsymbol{\gamma}\tilde{\nu}}}\,, \tag{3}$$

where $\boldsymbol{\epsilon}$ is the generic complex dielectric and *j* is an index over the vibrations (*Aj* is the strength, $\tilde{\boldsymbol{\nu}}_{\boldsymbol{0}}$ is the position, and $\boldsymbol{\gamma_j}$ is the full width at half maximum of each vibration). These results have been used as one of the calibrants for analyzing the composition of dust samples. Tables of the yeast cell and dielectric functions of other calibrants have been made available[22]. The ability to make quantitative absorption measurements under a microscope offers new avenues of analysis of microscopic-sized samples. This approach has been applied to inhalable dust.

5. INHALABLE DUST

Microparticles have great significance in health and science. The EPA invokes a 24 hr standard of 35 μg/m^3 for particulate matter smaller than 2.5 μm ($PM_{2.5}$) and an annual standard of 15 μg/m^3. Airborne particulate matter in the range of 2.5-10 μm ($PM_{10\text{-}2.5}$) includes the largest particles that get past our noses and throats making it into our lungs[23]. Since the airborne lifetime of particles decreases as the particle diameter increases, particles of ~4 μm diameter (the size trapped by our mesh) are expected to be correlated with both the local environment and health. It is desirable to know the chemical identity of components of particulate samples - an area where IR spectroscopy can be very useful. Increases in particulate matter are correlated with a large variety of diseases[24]. A dramatic illustration of this is the "London Smog" of Dec. 4-9, 1952, in which 7000 μg/m^3 of particulate matter (~300 times normal) is thought to have killed 12,000 people[24]. Airborne particles are mostly natural, but 6-23% are anthropogenic[24], and therefore diagnostic for human effects on the environment. Dust from space is collected to learn about the universe[25-27].

We have collected airborne dust from our lab air by pumping air through the plasmonic mesh[4] (see Figure 1). We have also collected dust from a household filter by shaking out dust and applying it to the mesh as air was pumped through. Libraries of scatter-free IR spectra of more than sixty individual, ~4μm particles from both the lab air[4] and a household filter were recorded. In order to analyze for the components, we have recorded sets of individual spectra of many materials as calibrants that were known to be in the lab air dust including calcite, dolomite, three types of clay, gypsum, polyethylene, yeast, and quartz[22]. A Mie-Bruggeman model has been presented that predicts the IR spectra of single particles that are variable mixtures of many different materials. The analytical accuracy of the model has yet to be determined, but it makes quantitative predictions. The individual spectra of each type of calibrant were averaged and fit to a Mie model (as described above for yeast) yielding a dielectric function with vibrations for each calibrant (like eq. 3). Given a set of volume fractions, f_i, for each calibrant, an initial guess of the effective dielectric of the mixture is made as $\epsilon_{eff_o} = \sum_{i=0}^{n-1} f_i \epsilon_i$, where ϵ_i is the dielectric function of each calibrant. Then, an iterative equation (indexed by *k*) was derived from the Bruggeman relation which refines the guess as:

$$\varepsilon_{eff,k} = \frac{\sum_{i=0}^{n-1} \frac{f_i \varepsilon_i}{\varepsilon_i + 2\varepsilon_{i,k-1}}}{\sum_{i=0}^{n-1} \frac{f_i}{\varepsilon_i + 2\varepsilon_{i,k-1}}} \quad . \tag{4}$$

Ten iterations are generally sufficient to obtain an effective dielectric function of the mixture. This approach was used with a nonlinear least squares routine to optimize the volume fractions. The best fits are shown in Figure 11 and the volume fractions are given in Table 1. The fits are promising, but more calibrants are likely needed to improve the situation. The two most striking differences in the two samples are that there is more organic material in the house filter dust and less quartz. There is no problem in adding new calibrants to the model and work is currently directed at getting calibrations for humic acid and its conjugate salt. One can imagine many other groups of organics that might help.

The use of individual particles exhibit crystalline orientation effects that are averaged away in powders or samples pressed into pellets. Also, lineshape distortions associated with the strong vibrations of dust particles in this size range exhibits much non-Beers law behavior[21]. The nonlinearities of this are largely unexplored with regard to

quantitative analysis. In the future we plan to study other dust samples, including dust from the World Trade Center 9/11/2001 event and dust collected by vacuuming at the International Space Station. Finally, there are plans to develop an anisotropic version of the Mie-Bruggeman model. This will enable the orientation of transition moments to be included in the model which will enable the modeling of single, mixed composition particles.

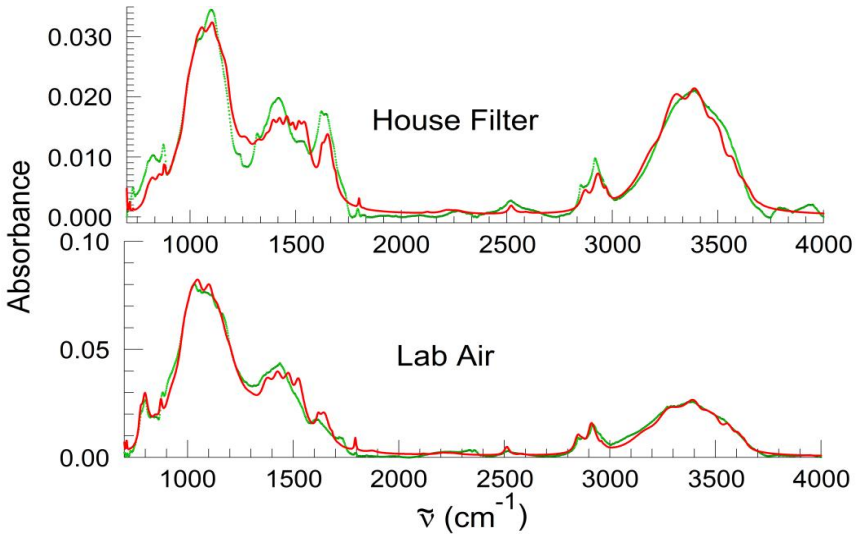

Figure 11. Average of all individual IR spectra from a library of lab air particles and a library of particles from a household filter. Each spectrum was fit with a Mie-Bruggeman model to determine the volume fractions of various components.

Table 1. Volume fractions of various calibrants in Lab Air and Household Filter collections.

Calibrant	House Filter Volume Fraction	Lab Air Volume Fraction
yeast	0.393	0.186(7)
illite	0.249	0.300(10)
gypsum	0.232	0.137(7)
calcite	0.079	0.103(2)
polyethylene	0.022	0.081(5)
dolomite	0.020	0.006(2)
quartz	0.000	0.186(6)
montmorillonite	0.000	0.000(12)
kaolinite	0.000	0.000(6)

ACKNOWLEDGEMENTS

We thank the National Science Foundation for support of this work under grant number CHE 1213293.

REFERENCES

[1] Garcia-Vidal, F. J., Martin-Moreno, L., and Pendry, J. B., "Surfaces with holes in them: new plasmonic metamaterials," Journal of Optics A: Pure and Applied Optics, 7, S97-S101 (2005).

[2] Martin-Moreno, L., Garcia-Vidal, F. J., Lezec, H. J. *et al.*, "Theory of Extraordinary Optical Transmission through Subwavelength Hole Arrays," Phys. Rev. Lett., 86(6), 1114-1117 (2001).

[3] Malone, M. A., McCormack, M., and Coe, J. V., "Single Airborne Dust Particles using Plasmonic Metal Films with Hole Arrays," J. Phys. Chem. Lett., 3(6), 720-724 (2012).

[4] Cilwa, K. E., McCormack, M., Lew, M. *et al.*, "Scatter-Free IR Absorption Spectra of Individual, 3-5 Micron, Airborne Dust Particles Using Plasmonic Metal Microarrays: A Library of 63 Spectra," J. Phys. Chem. C, 115(34), 16910-16919 (2011).
[5] Malone, M. A., Prakash, S., Heer, J. M. *et al.*, "Modifying Infrared Scattering Effects of Single Yeast Cells with Plasmonic Metal Mesh," J. Chem. Phys., 133(18), 185101-7 (2010).
[6] Heer, J., Corwin, L., Cilwa, K. *et al.*, "Infrared Sensitivity of Plasmonic Metal Films with Hole Arrays to Microspheres In and Out of the Holes," J. Phys. Chem. C, 114, 520-525 (2010).
[7] Ebbesen, T. W., Lezec, H. J., Ghaemi, H. F. *et al.*, "Extraordinary optical transmission through sub-wavelength hole arrays," Nature (London), 391(6668), 667-669 (1998).
[8] Schroter, U., and Heitmann, D., "Surface-plasmon-enhanced transmission through metallic gratings," Phys. Rev. B: Condens. Matter, 58(23), 15419-15421 (1998).
[9] Ulrich, R., "Far-infrared properties of metallic mesh and its complementary structure," Infrared Phys., 7(1), 37-55 (1967).
[10] Coe, J. V., Heer, J. M., Teeters-Kennedy, S. *et al.*, "Extraordinary Transmission of Metal Films with Arrays of Subwavelength Holes," Annu. Rev. Phys. Chem., 59, 179-202 (2008).
[11] Coe, J. V., Rodriguez, K. R., Teeters-Kennedy, S. *et al.*, "Metal films with Arrays of Tiny Holes: Spectroscopy with Infrared Plasmonic Scaffolding," J. Phys. Chem. C, 111(47), 17459-17472 (2007).
[12] Garcia-Vidal, F. J., Martin-Moreno, L., Ebbesen, T. W. *et al.*, "Light passing through subwavelength apertures," Rev. Mod. Phys., 82(1), 729-787 (2010).
[13] Genet, C., and Ebbesen, T. W., "Light in Tiny Holes," Nature (London, United Kingdom), 445, 39-46 (2007).
[14] Malone, M. A., Cilwa, K. E., Luthra, A. *et al.*, "Plasmonics under the Infrared Microscope: Sensing and Spectra of Single Particles Using Metal Film Hole Arrays," Photonics and Optoelectronics (SOPO), 2012 Symposium on 1(6), 21-23 (2012).
[15] Vigoureux, J. M., "Analysis of the Ebbesen experiment in the light of evanescent short range diffraction," OptCo, 198(4-6), 257-263 (2001).
[16] Malone, M. A., Cilwa, K. E., McCormack, M. *et al.*, "Modifying an Infrared Microscope To Characterize Propagating Surface Plasmon Polariton-Mediated Resonances," J. Phys. Chem. C, 115(25), 12250 (2011).
[17] Williams, S. M., and Coe, J. V., "Dispersion study of the infrared transmission resonances of freestanding Ni Microarrays," Plasmonics, 1(1), 87-93 (2006).
[18] Skorobogatiy, M., and Yang, J., [Fundamentals of Photonic Crystal Guiding] Cambridge University Press, (2009).
[19] van de Hulst, H. C., [Light Scattering by Small Particles] Dover, New York(1981).
[20] Bohren, C. F., and Huffman, D. R., [Absorption and Scattering of Light by Small Particles] Wiley-VCH Verlag GmbH, (2007).
[21] Ravi, A., Malone, M. A., Luthra, A. *et al.*, "Spectral Challenges of Individual Wavelength-Scale Particles: Strong Phonons and Their Distorted Lineshapes," Phys. Chem. Chem. Phys., 15(25), 10307-10315 (2013).
[22] Lioi, D. B., Cilwa, K. E., McCormack, M. *et al.*, "Infrared Spectral Model for Subwavelength Particles of Mixed Composition Based on the Spectra of Individual Particles with Calibration Data for Airborne Dust," The Journal of Physical Chemistry A, 117(44), 11297-11307 (2013).
[23] Hinds, W. C., [Aerosol Technology : Properties, Behavior, and Measurement of Airborne Particles] J. Wiley, New York (1982).
[24] Eastwood, P., [Particulate emissions from vehicles / by Peter Eastwood] John Wiley & Sons, Chichester, England ; Hoboken, NJ :(2008).
[25] Morlok, A., Bowey, J., Kohler, M. *et al.*, "FTIR 2-16 micron spectroscopy of micron-sized olivines from primitive meteorites," Meteorit. Planet. Sci., 41(5), 773-784 (2006).
[26] Morlok, A., Kohler, M., Bowey, J. E. *et al.*, "FT-IR microspectroscopy of extraterrestrial dust grains: Comparison of measurement techniques," Planet. Space Sci., 54(6), 599-611 (2006).
[27] Sandford, S. A., Aleon, J., Alexander, C. M. O. *et al.*, "Organics captured from comet 81P/Wild 2 by the Stardust spacecraft," Sci, 314(5806), 1720-1724 (2006).